Synthetic Gauge Field for Two-Dimensional Time-Multiplexed Quantum Random Walks

Hamidreza Chalabi,[1,2,*] Sabyasachi Barik,[1,2,3,†] Sunil Mittal,[1,2,‡] Thomas E. Murphy,[1,3,§] Mohammad Hafezi,[1,2,3,‖] and Edo Waks[1,2,3,¶]

[1]*Department of Electrical and Computer Engineering and Institute for Research in Electronics and Applied Physics, University of Maryland, College Park, Maryland 20742, USA*

[2]*Joint Quantum Institute, University of Maryland, College Park, Maryland 20742, USA*

[3]*Department of Physics, University of Maryland, College Park, Maryland 20742, USA*

(Received 17 February 2019; published 11 October 2019)

Temporal multiplexing provides an efficient and scalable approach to realize a quantum random walk with photons that can exhibit topological properties. But two-dimensional time-multiplexed topological quantum walks studied so far have relied on generalizations of the Su-Shreiffer-Heeger model with no synthetic gauge field. In this work, we demonstrate a two-dimensional topological quantum random walk where the nontrivial topology is due to the presence of a synthetic gauge field. We show that the synthetic gauge field leads to the appearance of multiple band gaps and, consequently, a spatial confinement of the quantum walk distribution. Moreover, we demonstrate topological edge states at an interface between domains with opposite synthetic fields. Our results expand the range of Hamiltonians that can be simulated using photonic quantum walks.

DOI: 10.1103/PhysRevLett.123.150503

Photonics provides a compelling platform to study quantum random walks [1]. Photons can propagate over long distances without losing coherence, enabling complex quantum walks that can implement various quantum computing algorithms [2–4] and also simulate a broad range of quantum Hamiltonians [5]. Photonic quantum walks in both one and two dimensions can be implemented in spatial degrees of freedom using beam splitters [6–8] or coupled waveguide arrays [9–11]. But such approaches are difficult to scale to a large number of steps, particularly when going to higher dimensions.

Synthetic spaces provide an alternative approach to scale the state space of the walker without requiring complex photonic circuits. Examples of synthetic spaces include frequency [12–16], orbital angular momentum [17–20], and transverse spatial modes as recently realized experimentally [21]. Time multiplexing is another synthetic space that is particularly easy to work with [22–27]. Time-multiplexed quantum walks have the advantage that they can span an extremely large state space with only a few optical elements and can efficiently scale to a higher number of walker dimensions.

Recently, time-multiplexed quantum walks have been used to explore topological physics and the associated edge states in both one- and two-dimensional systems [26,27]. Most realizations of such topological quantum walks are based on the split-step quantum walk protocol [28–31]. Similar to the Su-Shreiffer-Heeger model, here the nontrivial topology is a result of the direction-dependent hopping strength between the lattice sites. However, many of the most interesting topological Hamiltonians—such as the integer quantum Hall effect [32], the Haldane model [33], and the quantum-spin Hall effect [34]—require gauge fields that generate direction-dependent hopping phases. Synthetic gauge fields have been realized in a variety of physical systems [35–40] and also proposed in discrete-time quantum walks [41]. However, so far, time-multiplexed quantum walks with synthetic gauge fields have only been experimentally realized in one dimension, which severely restricts the scope of topological Hamiltonians that can be explored.

Here, we experimentally demonstrate a topological synthetic gauge field in a two-dimensional time-multiplexed quantum walk. We show that in our discrete-time quantum walk, the quasienergy band structure exhibits multiple band gaps depending on the magnitude of the synthetic gauge field. These band gaps result in the suppressed diffusion of the quantum walker, as opposed to ballistic diffusion that would otherwise occur [42]. Moreover, we demonstrate the presence of multiple topological edge bands at an interface between two domains with opposite magnetic fields. Because of the presence of two topological edge bands, our system supports two sets of nondegenerate topological edge states that travel in forward and backward directions along the interface.

To implement a gauge field, pulses must accumulate a net phase shift when walking around a closed trajectory. Figure 1(a) shows how we implement this condition. We apply a phase shift of $y\phi$ when the walker moves to the right and $-y\phi$ when the walker steps to the left, where y is the vertical coordinate of the walker. In this way, when walking around a closed trajectory, pulses will accumulate

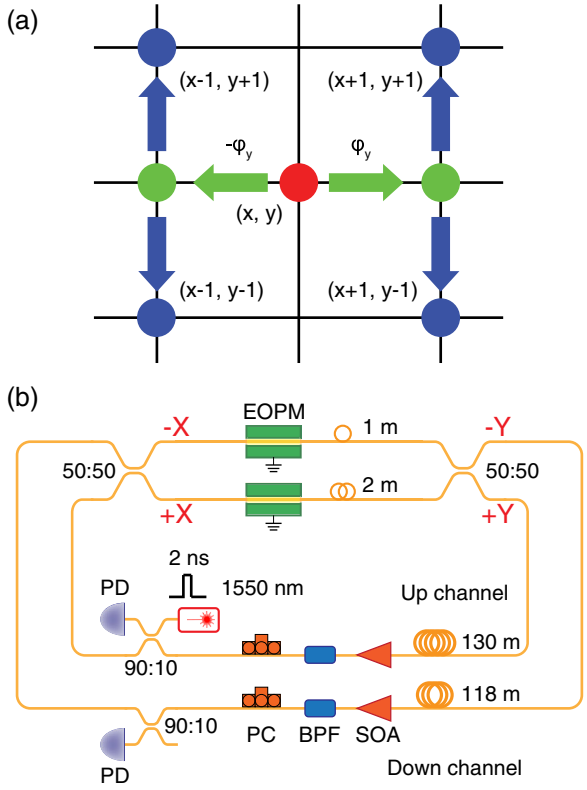

FIG. 1. (a) Schematic explaining the possible movements of a walker at spatial position (x, y) along with applied phase shifts during each step of the quantum walk. (b) Schematic of the two-dimensional quantum walk setup describing the details of the experimental setup. PD is for photodetector, BPF for band pass filter, SOA for semiconductor optical amplifier, EOPM for electro-optic phase modulator, and PC is for polarization controller.

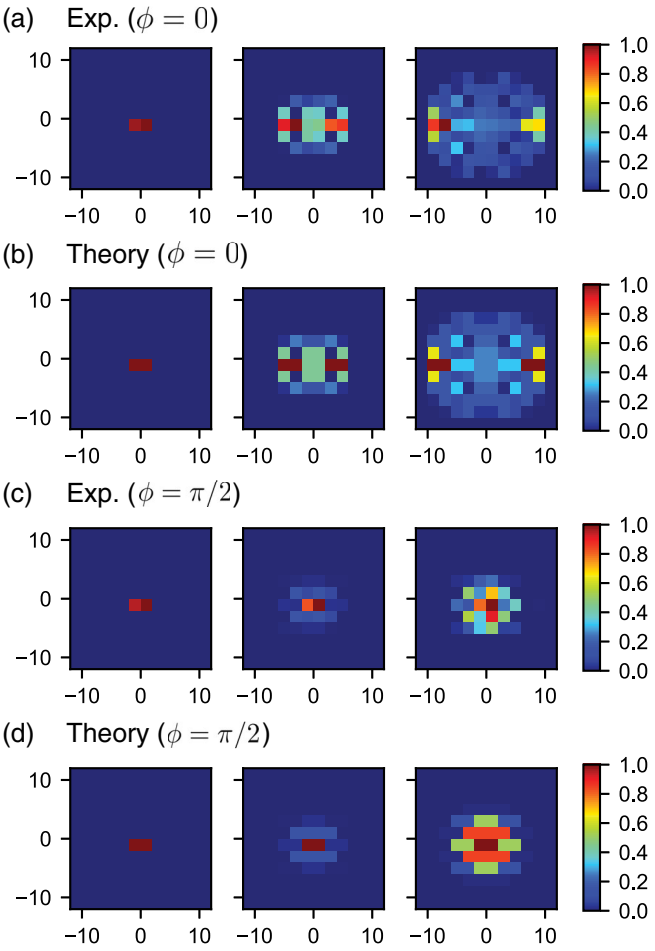

FIG. 2. (a) Experimental observations and (b) theoretical predictions of the evolution of the quantum walk distribution under no phase modulation. (c) Experimental observations and (d) theoretical predictions of the evolution of the quantum walk distribution under linearly dependent phase modulation $\phi_y = y\phi$ for the case of $\phi = \pi/2$. The left, middle, and right columns show the distributions at time steps of 1, 5, and 9, respectively. In these plots, all the distributions are normalized to their maximum.

a net phase proportional to the enclosed area. This phase convention realizes a uniform magnetic field in the Landau gauge. This type of phase pattern should be distinguished from the position-dependent but direction-independent phase shifts previously used for implementation of electric fields in discrete-time quantum walks [43–45].

In our time-multiplexed photonic quantum walk, optical delays map the walker state space into time delays of optical pulses. Similar to earlier studies [24,27] of two-dimensional quantum random walks, we implement these delays using a pair of nested fiber delay loops. Figure 1(b) shows the schematic of the experimental setup, and the full details are explained in the Supplemental Material [46]. The experimental setup consists of two beam splitters with their ports connected to fibers of different lengths such that they map the $\pm x$ and $\pm y$ directions to different time delays. One complete propagation of an optical pulse around the loop is then equivalent to hopping of the walker to one of the four possible corners in the synthetic space [Fig. 1(a)]. Two semiconductor optical amplifiers (SOAs) are employed to partially compensate for the losses that the optical pulses experience in each round trip. In this setup, we study the quantum walk distribution at each time step via two photodetectors analyzing two channels that we refer to as the up and down channels, as labeled in Fig. 1(b). We initialize the quantum walk through a single incident laser pulse that is injected into the up channel starting the evolution of the quantum walk distribution from the origin in synthetic space. Here, we have analyzed the evolution of the quantum walk based on the pulses detected in the down channel. The electro-optic modulators that are driven by programmable voltage waveforms are used for producing the desired phase shifts to generate the synthetic gauge field.

Figure 2 compares the evolution of the quantum walk distribution with and without an applied gauge field. Figure 2(a) shows the experimental results for the evolution under no applied gauge field. In this figure, the distribution of the quantum walker is shown at three different time steps of 1, 5, and 9. In the absence of a gauge field, the quantum walk exhibits rapid diffusion. These results are consistent

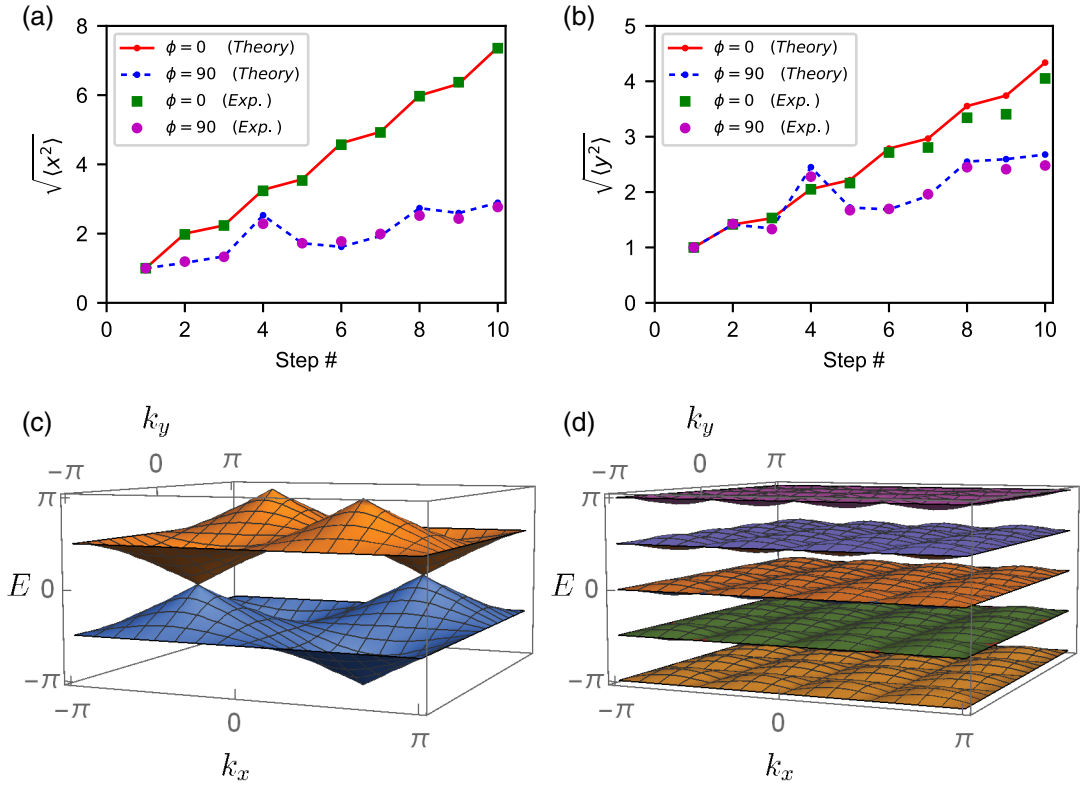

FIG. 3. (a) Comparison of the theoretical and experimental results for the variation of the quadratic mean of x under no gauge field as well as under the gauge field with $\phi = \pi/2$. (b) Comparison of the theoretical and experimental results for the variation of the quadratic mean of y under no gauge field as well as under the gauge field with $\phi = \pi/2$. The error bars in the measurements are smaller than the size of the plotted data points. (c,d) Band structure of the system under no phase modulation ($\phi = 0$) and a linear phase modulation ($\phi = \pi/2$).

with the theoretical predictions shown in Fig. 2(b). Figure 2(c) shows the experimental results for the evolution of the quantum walk distribution in the presence of a gauge field with $\phi = \pi/2$. The gauge field leads to suppressed diffusion and confinement of the quantum walk distribution. The experimental results shown in Fig. 2(c) for the case of a gauge field with $\phi = \pi/2$ are consistent with the theoretical predictions shown in Fig. 2(d).

We calculate the similarity of the measured distributions relative to the theoretical distributions (P_{th}) based on $F(n) = \sum_{x,y} \sqrt{P_{\text{th}}(x, y; n) P_{\text{exp}}(x, y; n)}$. For the case of no applied gauge field, we obtain similarities of 0.999, 0.996, and 0.985 for time steps of 1, 5, and 9, respectively. Similarly, for the quantum walk under the gauge field, we determine similarities of 0.999, 0.993, and 0.972 for time steps of 1, 5, and 9, respectively.

To provide a more quantitative analysis of the effect of the gauge field on the confinement of the quantum walk distribution, we calculate the variation of the spatial quadratic means as a function of the time step. Figures 3(a) and 3(b) plot the quadratic means of x and y with gauge fields of $\phi = 0$ and $\phi = \pi/2$. With no applied gauge field, the quadratic means show nearly linear variation with the time step, consistent with ballistic diffusion (see Supplemental Material [46] for an analytical explanation). But under the application of the gauge field with $\phi = \pi/2$, the quadratic means show reduced diffusion. The decrease of the quadratic means in both directions is due to the confinement of the quantum walk distribution under a constant pseudo-magnetic field. Figures 3(a) and 3(b) confirm the agreement of the experimental results with the theoretical predictions, both with and without the applied gauge field (see also Fig. S3 in the Supplemental Material [46] for the numerical study of the variation of quadratic means over a larger number of steps).

In order to better understand the confinement of the quantum walker in the presence of a gauge field, we first calculate the band structure of the quantum walk. The full evolution of the walker is determined by the single-step propagation matrix U, which advances the quantum walk distribution by one time step. According to Floquet band theory, the single-step propagation matrix determines the effective Hamiltonian from $U = e^{-iH_{\text{eff}}}$, which gives the band structure of the walker. With no synthetic gauge field ($\phi = 0$), we can analytically solve for the dispersion relation of the walker (see theoretical analysis section in the Supplemental Material [46]). The quasienergy bands of the system in this case are

$$E_{\pm} = \pm \arccos\left[\sin(k_x)\sin(k_y)\right], \tag{1}$$

where k_x and k_y are the momentum wave vectors in inverse synthetic space. Figure 3(c) shows the corresponding band structure of the system. Because of the discrete nature of the quantum walk, the quasienergy spectrum wraps every 2π, and therefore, we restrict the quasienergies to the range of $-\pi$ and π. As Fig. 3(c) shows, the system is gapless, and there are four Dirac points, two at $E = 0$ and two at $E = \pm\pi$.

We next consider the effect of the synthetic gauge field on the band structure. Figure 3(d) shows the band diagram for the case of $\phi = \pi/2$. An analytical solution for this case also exists (see Supplemental Material [46]), with a quasienergy band structure given by

$$E_{n,\pm} = \frac{n\pi}{2} \pm \frac{1}{4}\arccos\left(1 - \frac{1}{2}\sin^2(2k_x)\sin^2(2k_y)\right) \tag{2}$$

for $n \in \mathbb{Z}$. Similar to the case of the integer quantum Hall effect, the introduction of a gauge field produces a series of topological bands. For $\phi = \pi/2$, we observe four doubly degenerate bands. However, because of the wrapping of the quasienergy, one set of bands is split and appears close to energies $\pm\pi$. In contrast to the zero gauge field, the band structure in the presence of a synthetic gauge field exhibits band gaps that lead to the confinement of the quantum walker. We have also obtained the corresponding band diagrams for several other choices of ϕ. We have presented these results (see Fig. S2) along with their derivation in the Supplemental Material [46].

One consequence of a gauge field is the presence of edge states at the boundaries. In this synthetic space, we can make a boundary by applying two different gauge fields to two neighboring regions [41]. Here, using a phase modulation pattern of $\phi_y = y\phi$ for $y > 0$ and $\phi_y = -y\phi$ for $y < 0$, we realize two domains with opposite magnetic fields ($y > 0$ and $y < 0$), as illustrated in Fig. 4(a). Figure 4(b) shows the band structure for such a phase pattern with $\phi = \pi/2$. The band diagram contains multiple band gaps hosting unidirectional edge states that propagate at the boundary in opposite directions. The corresponding band diagrams for several other choices of ϕ are also presented in the Supplemental Material [46] (see Fig. S4).

Figure 4(c) shows experimentally measured results for the phase modulation pattern shown in Fig. 4(a). We start the quantum walker at the interface between the two magnetic domains, precisely where edge states should be present. In this case, the quantum walker predominantly walks along the edge, remaining confined to the boundary between the two regions. These results are consistent with the numerical simulations demonstrating how the edge states cause the quantum walk distribution to move mainly along the boundary [Fig. 4(d)]. We also note that because of the linear dispersion of the topological edge states

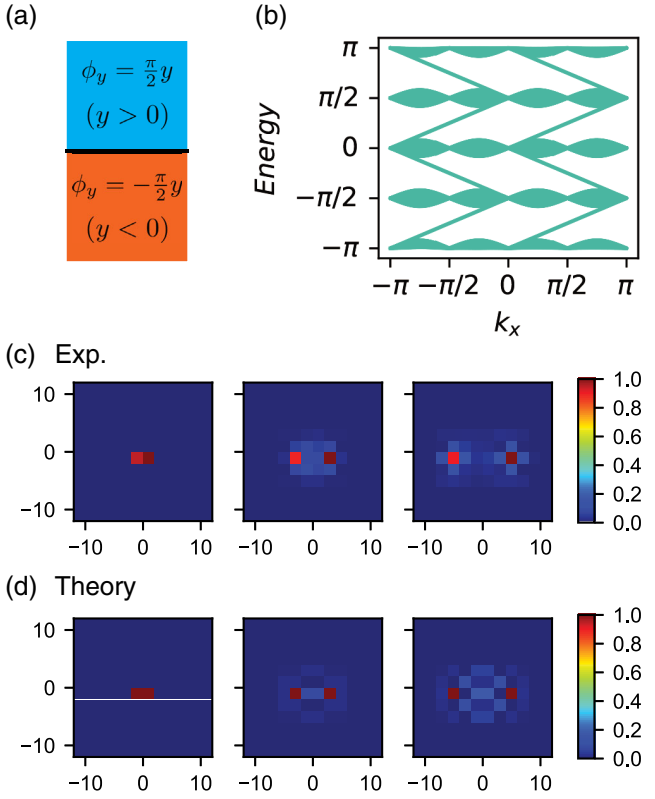

FIG. 4. (a) The schematic describing the phase modulation pattern of $\phi_y = |y|\phi$ for $\phi = \pi/2$ in the synthetic space. (b) Band diagram of the corresponding system, which clearly shows the presence of edge states in the band gap. (c) Experimental observations and (d) theoretical predictions of the evolution of the quantum walk distribution moving along the boundary under the phase modulation of $\phi_y = |y|\phi$ for $\phi = \pi/2$. The left, middle, and right columns show the distributions at time steps of 1, 5, and 9, respectively. In these plots, all the distributions are normalized to their maximum.

[see Fig. 4(b)], the photonic wave packets moving to the left and the right along the domain boundary experience minimal spreading [Fig. 4(c)], unlike that in the absence of edge states [Fig. 2(c)]. We have also studied the robustness of the edge modes against sharp bends in the Supplemental Material [46]. For this purpose, we have considered a nonplanar interface and have shown that the quantum walk distribution moves along the boundary and remains confined to it in spite of its nonplanar shape (see Fig. S5).

Typical topological quantum walks result in unidirectional edge-state propagation. Here, however, we do not see unidirectional movements because we are initializing the walker at a position eigenstate, which is a superposition of all energy eigenstates of the band structure. As can be seen from Fig. 4(b), different energy bands support topological edge states propagating in either the left or right direction. We could excite specific edge modes by engineering the initial distribution of the quantum walk to be confined in corresponding energies.

In conclusion, we have implemented time-multiplexed two-dimensional quantum random walks with a synthetic gauge field. This gauge field leads to the suppressed diffusion of the walker evolution. Through application of an inhomogeneous gauge field on this quantum walk, we observed the creation of topological edge states that are confined at the boundary of two distinct gauge fields. These results demonstrate a versatile approach to create various types of band structures with a tunable number of band gaps. In our setup, there exists an overall loss of around 6.5 dB in each round trip, and a major part (about 3 dB) of the loss comes from the fiber coupled modulators. In order to increase the number of steps, we used optical amplifiers to compensate for round-trip losses without damaging the phase coherence of the optical pulses. These losses can be reduced by decreasing coupler losses through fiber splicing and the use of modulators with lower insertion loss. Eliminating these losses opens up a path towards quantum random walks that can be implemented at the single photon level or in higher dimensions. The addition of optical nonlinearities and integration of this platform with single photon emitters could provide another interesting opportunity to study topological band structures with optical interactions [47,48]. Ultimately, our results expand the toolbox of quantum photonic simulation and provide a scalable architecture to study photonic quantum walks with nontrivial topologies.

This work was supported by the Air Force Office of Scientific Research-Multidisciplinary University Research Initiative (Grant No. FA9550-16-1-0323), the Physics Frontier Center at the Joint Quantum Institute, the National Science Foundation (Grant No. PHYS. 1415458), and the Center for Distributed Quantum Information. The authors would also like to acknowledge support from the U.S. Department of Defense. Moreover, the authors acknowledge support from the Laboratory for Telecommunication Sciences.

*hchalabi@umd.edu
†sbarik@umd.edu
‡mittals@umd.edu
§tem@umd.edu
‖hafezi@umd.edu
¶edowaks@umd.edu

[1] Y. Aharonov, L. Davidovich, and N. Zagury, Phys. Rev. A **48**, 1687 (1993).
[2] J. Kempe, Contemp. Phys. **44**, 307 (2003).
[3] N. Shenvi, J. Kempe, and K. B. Whaley, Phys. Rev. A **67**, 052307 (2003).
[4] A. M. Childs, R. Cleve, E. Deotto, E. Farhi, S. Gutmann, and D. A. Spielman, in *Proceedings of the Thirty-Fifth ACM Symposium on Theory of Computing—STOC '03* (ACM Press, New York, 2003), p. 59.
[5] A. M. Childs, D. Gosset, and Z. Webb, Science **339**, 791 (2013).
[6] F. De Nicola, L. Sansoni, A. Crespi, R. Ramponi, R. Osellame, V. Giovannetti, R. Fazio, P. Mataloni, and F. Sciarrino, Phys. Rev. A **89**, 032322 (2014).
[7] L. Sansoni, F. Sciarrino, G. Vallone, P. Mataloni, A. Crespi, R. Ramponi, and R. Osellame, Phys. Rev. Lett. **108**, 010502 (2012).
[8] M. A. Broome, A. Fedrizzi, B. P. Lanyon, I. Kassal, A. Aspuru-Guzik, and A. G. White, Phys. Rev. Lett. **104**, 153602 (2010).
[9] K. Poulios, R. Keil, D. Fry, J. D. A. Meinecke, J. C. F. Matthews, A. Politi, M. Lobino, M. Gräfe, M. Heinrich, S. Nolte, A. Szameit, and J. L. O'Brien, Phys. Rev. Lett. **112**, 143604 (2014).
[10] H. Tang, X.-F. Lin, Z. Feng, J.-Y. Chen, J. Gao, K. Sun, C.-Y. Wang, P.-C. Lai, X.-Y. Xu, Y. Wang, L.-F. Qiao, A.-L. Yang, and X.-M. Jin, Sci. Adv. **4**, eaat3174 (2018).
[11] H. Tang, C. Di Franco, Z.-Y. Shi, T.-S. He, Z. Feng, J. Gao, K. Sun, Z.-M. Li, Z.-Q. Jiao, T.-Y. Wang, M. S. Kim, and X.-M. Jin, Nat. Photonics **12**, 754 (2018).
[12] C. Navarrete-Benlloch, A. Pérez, and E. Roldán, Phys. Rev. A **75**, 062333 (2007).
[13] D. Bouwmeester, I. Marzoli, G. P. Karman, W. Schleich, and J. P. Woerdman, Phys. Rev. A **61**, 013410 (1999).
[14] Q. Lin, M. Xiao, L. Yuan, and S. Fan, Nat. Commun. **7**, 13731 (2016).
[15] Q. Lin, X.-Q. Sun, M. Xiao, S.-C. Zhang, and S. Fan, Sci. Adv. **4**, eaat2774 (2018).
[16] L. Yuan, M. Xiao, Q. Lin, and S. Fan, Phys. Rev. B **97**, 104105 (2018).
[17] S. K. Goyal, F. S. Roux, A. Forbes, and T. Konrad, Phys. Rev. Lett. **110**, 263602 (2013).
[18] F. Cardano, F. Massa, H. Qassim, E. Karimi, S. Slussarenko, D. Paparo, C. de Lisio, F. Sciarrino, E. Santamato, R. W. Boyd, and L. Marrucci, Sci. Adv. **1**, e1500087 (2015).
[19] F. Cardano, M. Maffei, F. Massa, B. Piccirillo, C. de Lisio, G. De Filippis, V. Cataudella, E. Santamato, and L. Marrucci, Nat. Commun. **7**, 11439 (2016).
[20] F. Cardano, A. D'Errico, A. Dauphin, M. Maffei, B. Piccirillo, C. de Lisio, G. De Filippis, V. Cataudella, E. Santamato, L. Marrucci, M. Lewenstein, and P. Massignan, Nat. Commun. **8**, 15516 (2017).
[21] E. Lustig, S. Weimann, Y. Plotnik, Y. Lumer, M. A. Bandres, A. Szameit, and M. Segev, Nature (London) **567**, 356 (2019).
[22] A. Schreiber, K. N. Cassemiro, V. Potoček, A. Gábris, P. J. Mosley, E. Andersson, I. Jex, and C. Silberhorn, Phys. Rev. Lett. **104**, 050502 (2010).
[23] A. Schreiber, K. N. Cassemiro, V. Potoček, A. Gábris, I. Jex, and C. Silberhorn, Phys. Rev. Lett. **106**, 180403 (2011).
[24] A. Schreiber, A. Gabris, P. P. Rohde, K. Laiho, M. Stefanak, V. Potocek, C. Hamilton, I. Jex, and C. Silberhorn, Science **336**, 55 (2012).
[25] T. Nitsche, F. Elster, J. Novotný, A. Gábris, I. Jex, S. Barkhofen, and C. Silberhorn, New J. Phys. **18**, 063017 (2016).
[26] S. Barkhofen, T. Nitsche, F. Elster, L. Lorz, A. Gábris, I. Jex, and C. Silberhorn, Phys. Rev. A **96**, 033846 (2017).
[27] C. Chen, X. Ding, J. Qin, Y. He, Y.-H. Luo, M.-C. Chen, C. Liu, X.-L. Wang, W.-J. Zhang, H. Li, L.-X. You, Z. Wang,

D.-W. Wang, B. C. Sanders, C.-Y. Lu, and J.-W. Pan, Phys. Rev. Lett. **121**, 100502 (2018).
[28] T. Kitagawa, M. S. Rudner, E. Berg, and E. Demler, Phys. Rev. A **82**, 033429 (2010).
[29] T. Kitagawa, E. Berg, M. Rudner, and E. Demler, Phys. Rev. B **82**, 235114 (2010).
[30] T. Kitagawa, M. A. Broome, A. Fedrizzi, M. S. Rudner, E. Berg, I. Kassal, A. Aspuru-Guzik, E. Demler, and A. G. White, Nat. Commun. **3**, 882 (2012).
[31] T. Kitagawa, Quantum Inf. Process. **11**, 1107 (2012).
[32] K. v. Klitzing, G. Dorda, and M. Pepper, Phys. Rev. Lett. **45**, 494 (1980).
[33] F. D. M. Haldane, Phys. Rev. Lett. **61**, 2015 (1988).
[34] M. Konig, S. Wiedmann, C. Brune, A. Roth, H. Buhmann, L. W. Molenkamp, X.-L. Qi, and S.-C. Zhang, Science **318**, 766 (2007).
[35] M. Hafezi, E. A. Demler, M. D. Lukin, and J. M. Taylor, Nat. Phys. **7**, 907 (2011).
[36] S. Mittal, J. Fan, S. Faez, A. Migdall, J. M. Taylor, and M. Hafezi, Phys. Rev. Lett. **113**, 087403 (2014).
[37] M. Aidelsburger, M. Lohse, C. Schweizer, M. Atala, J. T. Barreiro, S. Nascimbène, N. R. Cooper, I. Bloch, and N. Goldman, Nat. Phys. **11**, 162 (2015).
[38] P. Roushan *et al.*, Nat. Phys. **13**, 146 (2017).
[39] N. R. Cooper, J. Dalibard, and I. B. Spielman, Rev. Mod. Phys. **91**, 015005 (2019).
[40] T. Ozawa, H. M. Price, A. Amo, N. Goldman, M. Hafezi, L. Lu, M. C. Rechtsman, D. Schuster, J. Simon, O. Zilberberg, and I. Carusotto, Rev. Mod. Phys. **91**, 015006 (2019).
[41] M. Sajid, J. K. Asbóth, D. Meschede, R. Werner, and A. Alberti, Phys. Rev. B **99**, 214303 (2019).
[42] I. Yalcnkaya and Z. Gedik, Phys. Rev. A **92**, 042324 (2015).
[43] C. Cedzich, T. Rybár, A. H. Werner, A. Alberti, M. Genske, and R. F. Werner, Phys. Rev. Lett. **111**, 160601 (2013).
[44] L. A. Bru, M. Hinarejos, F. Silva, G. J. de Valcárcel, and E. Roldán, Phys. Rev. A **93**, 032333 (2016).
[45] M. Genske, W. Alt, A. Steffen, A. H. Werner, R. F. Werner, D. Meschede, and A. Alberti, Phys. Rev. Lett. **110**, 190601 (2013).
[46] See Supplemental Material at http://link.aps.org/supplemental/10.1103/PhysRevLett.123.150503 for methods and theoretical derivations.
[47] H. Chalabi and E. Waks, Phys. Rev. A **98**, 063832 (2018).
[48] H. Pichler and P. Zoller, Phys. Rev. Lett. **116**, 093601 (2016).